RSC Advances

PAPER

View Article Online
View Journal | View Issue

Cite this: *RSC Adv.*, 2019, **9**, 13696

Cylindrical shaped ZnO combined Cu catalysts for the hydrogenation of CO_2 to methanol

Hong Lei, Ruheng Zheng, Yeping Liu, Jiacheng Gao, Xiang Chen and Xiaoliang Feng*

Hydrogenation of CO_2 to chemicals is of great importance in the reduction of greenhouse gas emission. And the interaction and/or the boundary between Cu and ZnO played a crucial role in the performance of the Cu–ZnO catalyst for CO_2 hydrogenation to methanol. In this work, cylindrical shaped ZnO was first synthesized *via* controlled hydrothermal precipitation of $Zn(CO_2CH_3)_2 \cdot 2H_2O$, and Cu was further deposited on ZnO *via in situ* reduction in aqueous solution. Characterizations indicated that the crystallization degree of ZnO decreased with the increasing content of Cu, while the exposed surface area of Cu exhibited a volcano shaped curve. It was found that the cylindrical shaped ZnO combined Cu catalysts were active for the hydrogenation of CO_2, and the space time yield of methanol reached 0.50 $g_{\text{-MeOH}}$ $(g_{\text{-cat}}\ h)^{-1}$ at $H_2/CO_2 = 3$, 240 °C, 3.0 MPa, and 0.54 mol $(g_{\text{-cat}}\ h)^{-1}$, but the methanol selectivity decreases with the reduction of the (002) polar plane of ZnO. The conversion of CO_2 and methanol selectivity were discussed with the detected exposed Cu surface area and the number of oxygen vacancies.

Received 25th January 2019
Accepted 29th April 2019

DOI: 10.1039/c9ra00658c

rsc.li/rsc-advances

1. Introduction

The Paris Agreement, that dealing with greenhouse gas emission mitigation, was negotiated by representatives of 195 countries at the end of 2015. 194 members had signed and ratified the treaty in 2016. Among the greenhouse gases, the concentration of CO_2 in the atmosphere increased from 280 ppm in 1750 to 400 ppm in 2015. For this reason, an approach for efficient reduction of CO_2 has attracted the attention of scientists all over the world.[1–3] CO_2 recycling is one of the promising ways that will not only reduce CO_2 concentration but also produce some valuable chemicals like methanol, which is a key chemical feedstock and an alternative fuel.[4,5]

In published works, it was popularly accepted that Cu/ZnO-based catalysts were active for the hydrogenation of CO_2 to methanol,[6–11] and the activity of Cu-based catalysts depended mainly on the dispersion of Cu. However, the latest achievements disclosed that the interfacial area between Cu and ZnO played a crucial role for the activity and stability of the Cu/ZnO catalyst in methanol synthesis.[12–14] Cu/ZnO catalysts are usually prepared by co-precipitation using precipitation agents containing sodium,[8–11,15–18] while Kondrat *et al.* pointed out that residual sodium ions were a potential catalyst poison.[19] Therefore, the development of novel and effective techniques for preparing Cu/ZnO-based catalysts is of great importance.

Karelovic *et al.* found that Cu/ZnO catalysts prepared by combustion exhibited higher activity than those prepared *via* conventional coprecipitation methods, and the activity related to the contact between Cu and ZnO.[20] Valant *et al.*[21] reported that the activity of Cu/ZnO for methanol production changed with the content of Zn showed a volcano-like profile. Similar studies also confirmed that synergetic effect between Cu and ZnO could be responsible for the catalytic activity of Cu/ZnO catalysts in the synthesis of methanol from CO_2 hydrogenation.[7,9,22–28] Tsang *et al.*[7] disclosed that morphology of ZnO had a significant effect on its interaction with Cu in the hydrogenation of CO_2 to methanol. Plate-like ZnO showed a strong interaction with Cu, which leaded to high selectivity of methanol. Previous work in our laboratory also found that filament-like ZnO supported Cu catalyst was highly active for CO_2 hydrogenation,[11] which might be attributed to that filament-like ZnO possessed large polar plane, and the interaction between Cu and ZnO was strong. At the same time, Khanna *et al.*[29] developed a wet chemical reduction method to prepare nano-sized Cu particles, in which a reduction reaction occured between Cu^{2+} and reducing agent. This method is simple, easy in control and can prepare metallic Cu without further reduction.

In this work, cylindrical shaped ZnO was synthesized *via* controlled hydrothermal precipitation of $Zn(CO_2CH_3)_2 \cdot 2H_2O$, and Cu was further deposited on ZnO *via* the *in situ* reduction of Cu^{2+} with L-ascorbic acid in aqueous solution. The physicochemical properties of prepared Cu/ZnO were characterized by X-ray diffraction (XRD), scanning electron microscope (SEM), N_2 adsorption, N_2O chemisorption techniques, Raman spectra, X-

College of Chemical and Material Engineering, Quzhou University, Quzhou 324000, China. E-mail: 28826589@qq.com; Fax: +86-570-8015112; Tel: +86-570-8026546

ray photoelectron spectroscopy (XPS), H_2 and CO_2 chemisorption, H_2-TPD, and CO_2-TPD techniques. The relationship between the physiochemical properties of Cu/ZnO and its performance in hydrogenation of CO_2 was discussed.

2. Experimental section

2.1. Synthesis of cylindrical shaped ZnO

12.00 g of $Zn(CO_2CH_3)_2 \cdot 2H_2O$ (Aladdin, 99.99%) was dissolved in deionized water (240 mL), and then 7.32 g of diethylenetriamine (Aladdin, 99%) was added under vigorous stirring. After diethylenetriamine was dissolved, the solution was transferred into a 500 mL polytetrafluoroethylene-lined autoclave and kept at 97 °C for 24 h, and then cooled to room temperature. The precipitate was filtered and washed thoroughly with deionized water to remove excess precursor and dried at 60 °C for 12 h, and further calcined in air at 450 °C for 2 h.

2.2. Synthesis of Cu

20 mmol of $Cu(CO_2CH_3)_2 \cdot H_2O$ (Alfa Aesar, 99.9%) was dissolved in 50 mL of deionized water. The resulting solution was heated to 70 °C in an oil bath with magnetic stirring. A 60 mL of L-ascorbic acid (Alfa Aesar, ≥99%) aqueous solution (1.0 M) was added dropwise into the flask to reduce Cu^{2+} under vigorous stirring. The black precipitate was filtered and washed with ethanol, dried in vacuum at 60 °C for 12 h and stored in desiccator (in N_2).

2.3. Deposition of Cu on ZnO

$Cu(CO_2CH_3)_2 \cdot H_2O$ aqueous solution was prepared by dissolving 20 mmol of $Cu(CO_2CH_3)_2 \cdot H_2O$ in 50 mL of deionized water and then the as-prepared cylindrical shaped ZnO (10 mmol) was added. The resulting suspension solution was heated to 70 °C in an oil bath with magnetic stirring. A 60 mL of L-ascorbic acid aqueous solution (1.0 M) was added dropwise into the flask to reduce Cu^{2+} under vigorous stirring. After reaction, the black precipitate was filtered and washed with ethanol. The solid was dried in vacuum at 60 °C for 12 h and stored in desiccator (in N_2). The prepared catalyst was designated as CZ-2. CZ-1, CZ-3 and CZ-4 were also prepared in the same procedure (L-ascorbic acid/Cu^{2+} = 3, molar ratio) with different copper acetate amount, in which 1, 3 and 4 mean Cu/Zn molar ratio. For comparison, the Cu/ZnO catalyst (with a Cu/Zn atomic ratio of 2) was prepared by carbonate coprecipitation.[11] After hydrogen reduction at 270 °C for 2 h, the catalyst was identified as CA-CC.

2.4. Characterization

The composition of prepared catalysts was examined by inductively coupled plasma-atomic emission spectrometry (ICP, Plasma-Spec-II spectrometer), and the actual copper content in prepared catalysts was confirmed and summarized in Table 1.

XRD analysis was carried out on a Rigaku D/MAX-2500 diffractometer with a scanning angle of 15–85° by Cu Kα radiation. SEM images of these catalysts were obtained using Leo Series VP 1430 microscope operated at 10 kV. After samples were pretreated at 250 °C for 4 h in vacuum, N_2 adsorption was measured at −196 °C using an ASAP 2010 analyzer. Surface area was calculated according to the BET method, which used 0.164 nm^2 as the cross-sectional area of the nitrogen molecule. The metallic copper surface areas (S_{Cu}) were measured using a N_2O chemisorption method as described elsewhere.[30] The surface area of copper was calculated by assuming that the surface density of atomic copper was 1.46×10^{19} Cu atoms per m^2 and molar stoichiometry of N_2O/Cu was 0.5. Raman analysis was performed on a Jobin Yvon Labram HR800 spectrometer. XPS measurement was performed using a Mg Kα ray as excitation source ($h\nu$ = 1253.6 eV) on a PerkinElmer PHI 5000C system. Surface contamination of C 1s peak (284.6 eV) was used as internal standard calibration binding energy.

H_2 (or CO_2) chemisorption measurements were performed at 30 °C using a Micromeritics Autochem 2920 II apparatus. 0.30 g of the catalyst was loaded between two quartz wool balls into a quartz U-shaped tube reactor. The measurements were carried out by pulses injection (0.551 mL) of 10% H_2/Ar (or 10% CO_2/He) until saturation. Chemisorbed and physisorbed H_2 (or CO_2) consumption was monitored by a thermal conductivity detector (TCD), which was denoted A_{total}. The sample was then degassed with Ar (or He) for 10 min to evacuate physisorbed H_2 (or CO_2). Physisorbed H_2 (or CO_2) consumption was measured by another series of H_2 (or CO_2) pulses under the same conditions, which was denoted A_{phys}. The chemisorbed H_2 (or CO_2) was calculated as follows:

$$A_{chem} = A_{total} - A_{phys}$$

Table 1 Physicochemical properties of the ZnO, Cu and CZ catalysts

Catalysts	Cu/(Cu + Zn)[a] (mol%)	S_{BET} (m^2 g_{-cat}^{-1})	d_{Cu} (nm)	S_{Cu}[b] (m^2 g_{-cat}^{-1})
ZnO	0	7.8	—	—
CZ-1	49.2	23.7	9.6	8.2
CZ-2	66.3	35.5	7.3	12.3
CZ-3	74.4	26.3	13.2	9.6
CZ-4	79.6	21.2	14.1	7.4
CZ-CC	66.9	38.8	10.5	10.9
Cu	100.0	3.3	67.1	3.1

[a] Determined by ICP method. [b] Determined by N_2O chemisorption method.

where the unit of A is mol g^{-1}.

H_2 or CO_2 temperature-programmed desorption (H_2-TPD or CO_2-TPD) of catalysts were performed on Micromeritics Autochem 2920 II apparatus. H_2 or CO_2 stream was introduced for adsorption (30 min) at room temperature. After adsorption, the samples were flushed with Ar (H_2-TPD) or He (CO_2-TPD) stream (30 mL min^{-1}) for 30 min to remove weakly adsorbed H_2 or CO_2, and then they were heated from 20 to 700 °C at a rate of 10 °C min^{-1}. The desorbed H_2 or CO_2 was detected by TCD.

2.5. Catalyst reactions

The activity of the catalyst was tested in a continuously flowing fixed-bed reactor (MRCS8004). 1.0 g of the catalyst diluted with quartz sand (both in 20–40 mesh) was charged into a stainless steel tubular reactor. Then, CO_2 (99.9%) and H_2 (99.9%) was introduced. The reaction conditions used in the activity test were 240 °C, 3.0 MPa, 0.54 mol $(g_{\text{-cat}}\ h)^{-1}$ and molar feed composition of $CO_2/H_2 = 1/3$. All post reactor lines and valves were heated to 150 °C to prevent product condensation. The products were analyzed online by gas chromatography (Agilent 6820). Methanol was measured by a flame ionization detector with a Porapak-Q column and other gaseous products were analyzed by a thermal conductivity detector with a Carbosieve column. The conversion and selectivity values were calculated as the average of three different analyses performed after 2 hours of flow operation.

3. Results and discussion

3.1. Structure of the catalysts

Cu content in prepared catalysts was determined in ICP and summarized in Table 1. The real content of Cu was quite close to the theoretical values, indicating that the composition of CZ catalysts *via in situ* chemical reduction could be precisely controlled.

Fig. 1a shows the XRD patterns of cylindrical shaped ZnO prepared by the hydrothermal synthesis method and Cu obtained with chemical reduction method. All diffraction peaks of ZnO could be ascribed to wurtzite ZnO, and no other impurity peaks was observed. These results indicated that mainly well crystallized ZnO was formed in the hydrothermal reaction. It can be found that the diffraction lines of Cu appeared at $2\theta = 43.1°$ and $50.2°$. These data confirmed that the Cu^{2+} was reduced to metallic Cu by L-ascorbic acid in the aqueous solution.

Fig. 1b and c show the XRD patterns of CZ catalysts with different Cu/ZnO molar ratios obtained by *in situ* reduction reaction and carbonate coprecipitation. The diffraction peak of Cu (111) was weakened and broadened when Cu/Zn molar ratio was less than 2, which implied that crystallite size of Cu was small. In contrast, the diffraction peaks of Cu enhanced when the molar ratio Cu/Zn increased to 4, which meant that the crystallite size of Cu would be large. Similar phenomena were also reported by Lee *et al.*[31] The average crystallite size of Cu was calculated using Scherrer's equation and summarized in Table 1. It can be found that the crystallite size of Cu was 67.1, 9.6, 7.3, 13.2, 14.1 and 10.5 nm in Cu, CZ-1, CZ-2, CZ-3, CZ-4 and CZ-CC, respectively, which indicated that ZnO could promote the dispersion of Cu. Another interesting observation was that the diffraction intensity of ZnO decreased gradually with the

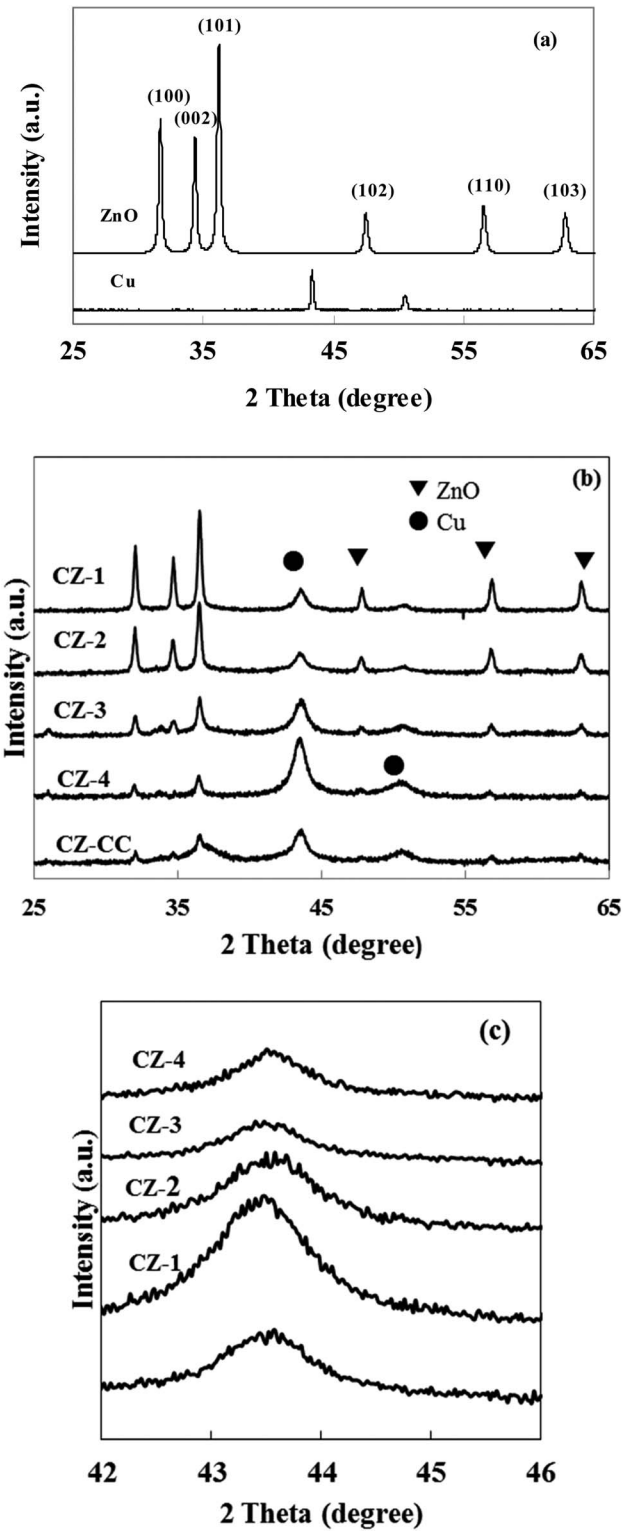

Fig. 1 XRD patterns of cylindrical shaped ZnO, Cu and CZ catalysts. (a) Cylindrical shaped ZnO and Cu; (b) CZ catalysts; (c) Cu (111).

increase of Cu content. The diffraction peak of polar (002) plane of ZnO disappeared and only wide and weak diffraction peaks of nonpolar (001) and (101) planes were observed over CZ-4, which suggested that the polarity and crystallite size of ZnO decreased with the increase of Cu content. The diffraction peak of (002) plane of ZnO over CZ-CC was also weak, which suggested that the polarity of ZnO was also weak. Zhu *et al.*[32] found that plate-like ZnO possessed mostly polar (002) faces contained more oxygen vacancies, while rod-like ZnO had mostly nonpolar (101) faces contained less oxygen vacancies.

Fig. 2a shows the SEM image of ZnO sample prepared by controlled hydrothermal precipitation of $Zn(CO_2CH_3)_2 \cdot 2H_2O$. The diameter of cylindrical shaped ZnO is about 7 μm. Fig. 2b is the image of Cu prepared by chemical reduction method. It reveals that the shape of Cu is sphere-like with diameter of 3 μm. Interestingly, when ZnO was used as carrier for heterogeneous nucleation and growth of Cu, different shapes of Cu were observed, ranging from sphere to irregular shape (Fig. 2c–e). The result demonstrates that there is strong interaction between Cu and ZnO. The particle sizes of Cu over CZ catalysts are also smaller than pure Cu, implying that ZnO can promote the dispersion of Cu.

Fig. 2c–e are the images of CZ-1, CZ-2 and CZ-4 prepared by a *in situ* chemical reduction reaction. An increase in Cu content

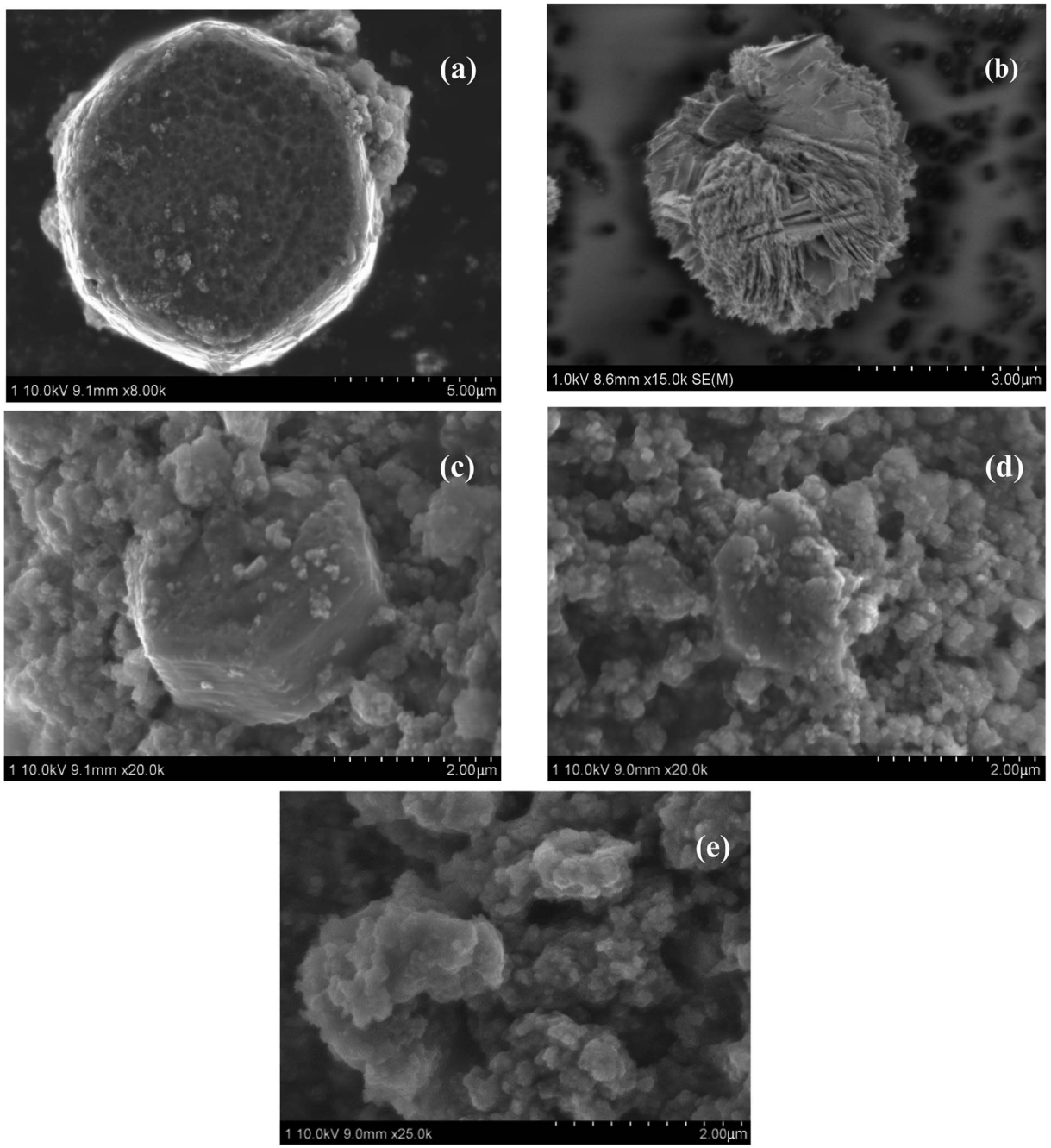

Fig. 2 SEM images of cylindrical shaped ZnO, Cu and CZ catalysts. (a) Cylindrical shaped ZnO; (b) Cu; (c) CZ-1; (d) CZ-2; (e) CZ-4.

leaded to a change in particle size of Cu. The minimum particle size was obtained for CZ-2, and then an increase in particle size of Cu appeared for CZ-4. This result was in accordance with the result of XRD. Furthermore, it can be seen from Fig. 2c–e that the particle size of cylindrical shaped ZnO decreased with the increase in the Cu content and ZnO was coated with large amount of Cu over CZ-4. The result also correlated well with the result of XRD.

Fig. 3 shows Raman spectra of catalysts with different copper loading. The Raman shift at around 323 cm^{-1} belonged to the E_{2H}–E_{2L} phonon mode of ZnO, and another peak at around 428 cm^{-1} was attributed to the high frequency optical phonon mode (E_{2H}) of ZnO.[33] The characteristic peaks of Raman spectra indicated that ZnO was in the form of wurtzite structure. Fig. 3 also confirmed that the position, width and intensity of E_{2H}–E_{2L} and E_{2H} peaks changed obviously with the increasing content of Cu. The position of peak shifted to low wave number, width of peak broadened and its intensity became small, which indicated that Cu contacted strongly with ZnO.[33,34]

The BET surface area and exposed Cu surface area in pure Cu, ZnO and CZ catalysts were summarized in Table 1. The exposed Cu surface area of CZ catalysts was higher than that of pure Cu, which indicated that ZnO could dispersed Cu. It can be also found that surface area of Cu/ZnO catalyst prepared by *in situ* chemical reduction reaction passed its maximum (35.5 m^2 $g_{\text{-cat}}^{-1}$, in CZ-2) and then decreased slightly with the increasing content of Cu, and the detected surface area of exposed Cu exhibited in a similar tendency. However, both BET surface area and exposed Cu surface area reduced progressively with high Cu loadings, which could be due to copper agglomeration at Cu/Zn molar ratio > 2. CZ-2 had the largest BET surface area (35.5 m^2 $g_{\text{-cat}}^{-1}$) and the largest exposed Cu surface area (12.3 m^2 $g_{\text{-cat}}^{-1}$). These results showed that the Cu/Zn ratio could influence the BET surface area and exposed Cu surface area. It can be also found from Table 1 that CZ-2 prepared by *in situ* chemical reduction reaction has larger exposed Cu surface areas than that obtained by carbonate coprecipitation, which correlated well with Cu crystallite size.

Fig. 4 shows the XPS date of CZ-1, CZ-2 and CZ-4 catalysts obtained by *in situ* chemical reduction reaction. Fig. 4a reveals that the binding energy value of O 1s for CZ-1 (528.9 eV) is lower than that of CZ-2 (529.7 eV) and CZ-4 (530.2 eV), implying that electrons are easier to be excited from ZnO over CZ-1 and ZnO over CZ-1 has more oxygen vacancies.[11] From Fig. 4a, it is found that O 1s XPS band can be decomposed into low binding energy peak and high binding energy peak, which are attributed to lattice oxygen (O_{latt}) and oxygen vacancies (O_{vac}), respectively.[35,36] With the increase of copper content, the O_{vac}/O_{latt} molar ratio decreases gradually. The result indicates that CZ-1 has more oxygen vacancies. The binding energy value of Cu $2p_{3/2}$ of CZ catalysts is shown in Fig. 4b. It can be found that the binding energy value of Cu $2p_{3/2}$ of CZ-1 is lower than that of CZ-2 and CZ-4 catalysts. The [O] terminated polar (002) facet is known to be electron richer than those of nonpolar facets (*i.e.* 100) that contain equal number of cations and anions.[7] The

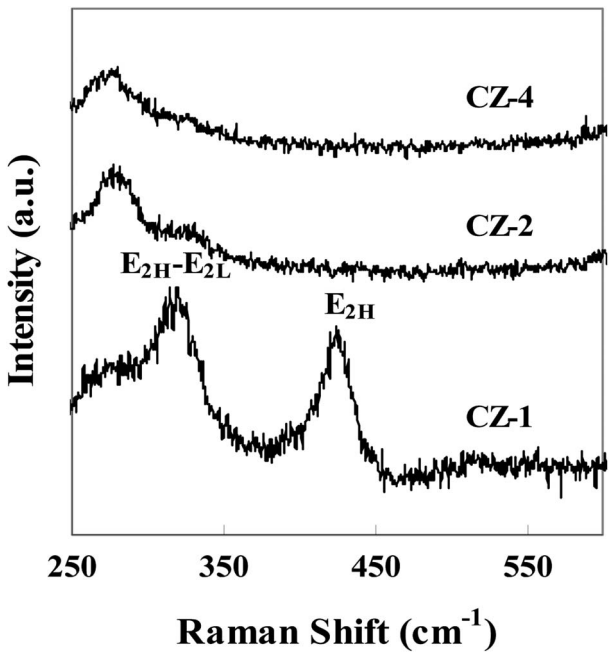

Fig. 3 Raman spectra of CZ catalysts.

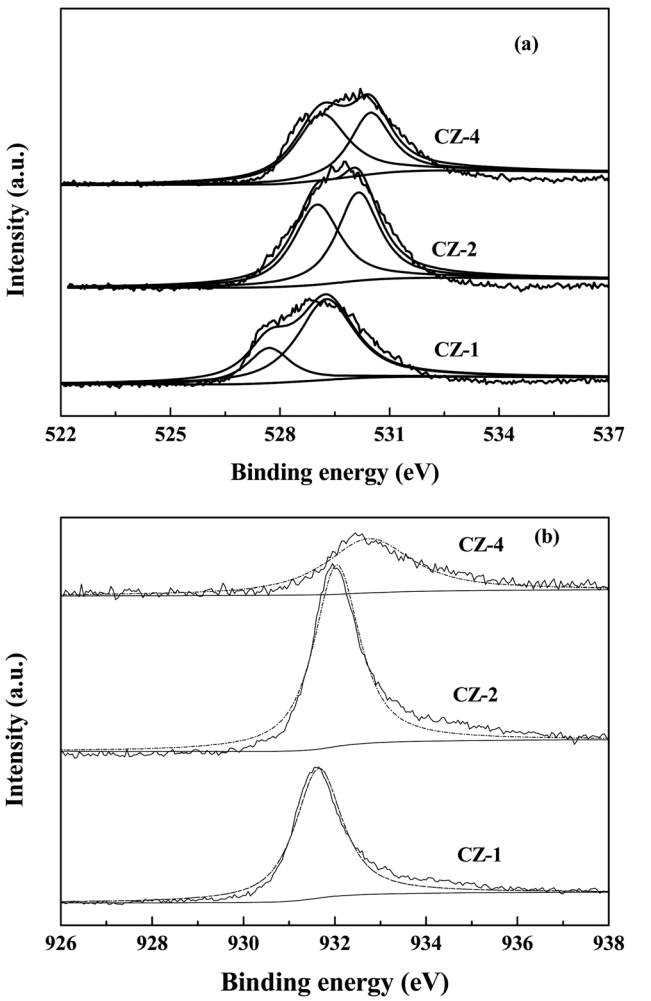

Fig. 4 XPS patterns of CZ catalysts. (a) O 1s in CZ catalysts; (b) Cu $2p_{3/2}$ in CZ catalysts.

XRD result has demonstrated that reflection of polar (002) facet of ZnO reduces with the increase of Cu content, implying that electrons are easier to transfer from ZnO over CZ-1 to Cu.

Fig. 5a shows that when the Cu content increases, the amount of chemisorbed CO_2 decreases, and bare Cu does not adsorb CO_2. The observation indicates that adsorbed CO_2 amount is inversely proportional to the Cu content since the addition of Cu decreases the basicity of the catalyst and therefore is not in favor of the adsorption of acidic CO_2. However, this decrease is slower than what can be expected from a linear trend (Fig. 5a, dotted lines). This indicates that the basicity of ZnO in catalysts has been increased with increase of Cu content, which is in agreement with the amount of oxygen vacancies (the Lewis basicity is increased in the absence of vacancies). Hydrogen chemisorption experiments are shown in Fig. 5b. It can be found that hydrogen is weakly chemisorbed on pure Cu since Cu is known to quickly decompose and recombine hydrogen.[37] However, ZnO can adsorb atomic H through hydrogen spillover,[21,38] which leads a strong adsorption. When the ZnO content increases, a volcano-type profile is observed showing a maximum of chemisorbed hydrogen for CZ-2. This shape is characteristic of a synergetic effect where the combination of Cu and Zn permits a significant increase of adsorbed hydrogen. This evolution matches exposed Cu surface area. The investigation of CO_2 and H_2 chemisorption suggests that both Cu and ZnO are active sites.

Fig. 6 shows the H_2-TPD patterns of CZ-1, CZ-2 and CZ-4 catalysts obtained by *in situ* chemical reduction reaction. For comparison, the CZ-CC catalyst obtained by carbonate coprecipitation was also investigated. It is found that all samples display a H_2 desorption peak in the range of 120–300 °C, which is assigned to the desorption of atomic hydrogen adsorbed on the surface of metallic Cu sites.[39] Another strong H_2 desorption peak located in the range of 450–600 °C is also discovered for all samples. It represents the desorption of strongly-adsorbed hydrogen on the ZnO surface through spillover from Cu to

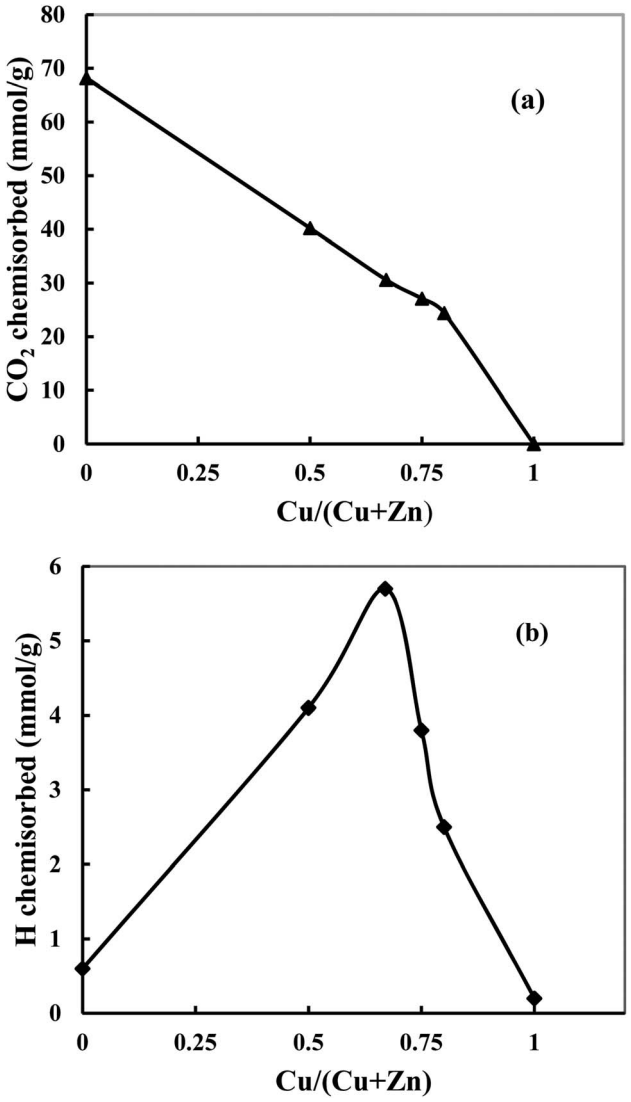

Fig. 5 Chemisorbed CO_2 (a) and hydrogen (b) as a function of Cu content in the catalyst.

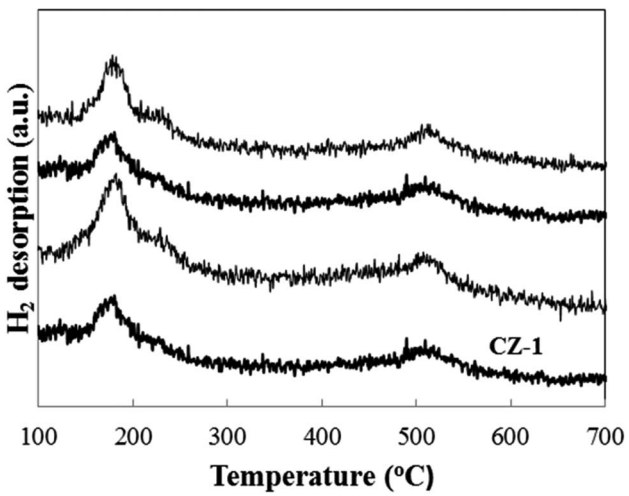

Fig. 6 H_2-TPD profiles of the CZ catalysts.

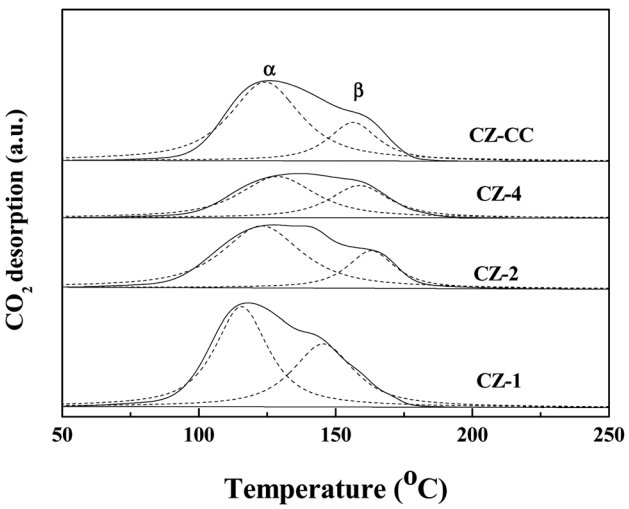

Fig. 7 CO_2-TPD profiles of the CZ catalysts.

ZnO.[39] From Fig. 6, it is found that the maximum H_2 desorption amount is obtained for CZ-2 with increase in Cu content. Under the same Cu/Zn molar ratio, the H_2 desorption amount CZ-2 is larger than that over CZ-CC. This result matches exposed Cu surface area.

Fig. 7 shows the CO_2 desorption profiles of CZ-1, CZ-2, CZ-4 and CZ-CC catalysts. From CO_2-TPD results, it can be observed that all profiles can be deconvoluted into two Gaussian peaks, which can be assigned to the weakly-adsorbed CO_2 on the weak basic sites and strongly-adsorbed CO_2 on the strong basic sites, respectively. The CO_2 adsorption capacity order of CZ catalysts as follows: CZ-1 > CZ-CC > CZ-2 > CZ-4. The result indicates that the addition of Cu decreases the basicity of the catalyst. CZ-CC has stronger basicity than CZ-2 under the same ZnO content, which can be attributed to fewer oxygen vacancies.

3.2. Catalytic performance

The catalytic activity and selectivity of these catalysts for CO_2 hydrogenation to methanol are summarized in Table 2. Methanol and CO are the only carbon-containing products under the reaction conditions. It can be seen that the conversion of CO_2 increased with increasing Cu/Zn molar ratio from 0 to 2. However, when the Cu content was increased further, the conversion of CO_2 decreased. If bare Cu was used, no CO_2 conversion was observed. These results indicated that bare Cu did not adsorbed CO_2. CZ-2 catalyst exhibited the best activity for CO_2 hydrogenation with a 17.8% conversion of CO_2. The calculated space time yield (STY) of CZ-2 reached maximum of 0.50 $g_{\text{-MeOH}}$ $(g_{\text{-cat}}\ h)^{-1}$, while STY decreased to 0.18 $g_{\text{-MeOH}}$ $(g_{\text{-cat}}\ h)^{-1}$ over CZ-4. The conversion of CO_2 and STY decreased to 13.2% and 0.28 $g_{\text{-MeOH}}$ $(g_{\text{-cat}}\ h)^{-1}$ over CZ-CC. Under the same reaction conditions, STY was 0.24 $g_{\text{-MeOH}}$ $(g_{\text{-cat}}\ h)^{-1}$ over the CZ catalyst prepared by conventional carbonate co-precipitation method.[11] Gao *et al.*[39] reported that STY was 0.34 $g_{\text{-MeOH}}$ $(g_{\text{-cat}}\ h)^{-1}$ over the $Cu/ZnO/Al_2O_3$ prepared by the co-precipitation method (reaction conditions: $H_2/CO_2 = 3$, $T = 250$ °C, $P = 5.0$ MPa, GHSV = 0.54 mol $(g_{\text{-cat}}\ h)^{-1}$). As well known, for Cu-based catalysts, a larger exposed Cu surface area results in a higher catalytic activity.[40,41] The amount of chemisorbed hydrogen increases with increase of exposed Cu surface area, which leads to higher CO_2 conversion. At the same time, the results of N_2O chemisorption measurements suggested that the exposed Cu surface area increased firstly and then decreased with the increase of Cu content. CZ-2 catalyst exhibited the largest exposed Cu surface area.

Furthermore, it is noteworthy that a remarkable decrease in methanol selectivity can be observed with the increase in Cu content. The value of methanol selectivity over CZ-4 was 48.3%, which decreased by about 47% relative to ZnO (91.2%). This result was consistent with the reduction of oxygen vacancies. Hydrogen was spilled on ZnO and ZnO_x (oxygen vacancies) by hydrogen spillover phenomenon[9] where CO_2 was adsorbed. We supposed that atomic H adsorbed on ZnO reacted with CO_2 to produce CO, while atomic H adsorbed on ZnO_x reacted with CO_2 to synthesize methanol.

Table 2 shows the effect of Cu loading on TOF value of methanol over CZ catalyst. The TOF value of methanol decreased with the increase of Cu/Zn molar ratio. These results indicated that the CZ catalyst was a structural sensitive catalyst for methanol synthesis from CO_2 hydrogenation. Tsang *et al.*[7] proposed that Cu/ZnO catalyst had double active centers: one was Cu, and another was the oxygen vacancy on the interface of the Cu–Zn. In our experiment, the increase of Cu loading led to the decrease of TOF value of methanol, which was attributed to reduction of oxygen vacancy between Cu–Zn interface leading to the decrease of methanol selectivity. In view of the above, we presented that the mechanism of CO_2 hydrogenation over Cu/ZnO catalysts could be described as follows: firstly, the

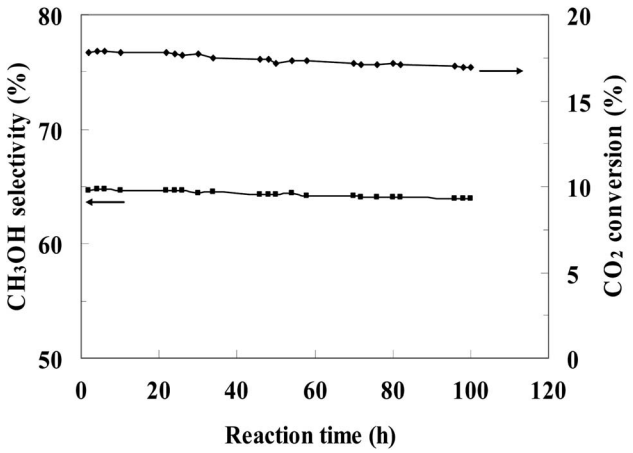

Fig. 8 Stability of CZ-2 for the CO_2 hydrogenation process. (Reaction conditions: $H_2/CO_2 = 3$, $T = 240$ °C, $P = 3.0$ MPa, GHSV = 0.54 mol $(g_{\text{-cat}}\ h)^{-1}$).

Table 2 Performance for the hydrogenation of CO_2 over ZnO, Cu and CZ catalysts[a]

Catalysts	CO_2 conversion (%)	CH_3OH selectivity (%)	STY ($g_{\text{-MeOH}}$ $(g_{\text{-cat}}\ h)^{-1}$)	TOF of CH_3OH $\times 10^3$ (s^{-1})
ZnO	0.2	91.2	0.01	—
CZ-1	11.9	71.5	0.37	17.0
CZ-2	17.8	64.7	0.50	15.4
CZ-3	12.6	54.2	0.30	11.7
CZ-4	8.7	48.3	0.18	9.4
CZ-CC	13.2	49.9	0.28	9.5
Cu	0.0	0.0	0.00	0.0

[a] Reaction conditions: $H_2/CO_2 = 3$, $T = 240$ °C, $P = 3.0$ MPa, GHSV = 0.54 mol $(g_{\text{-cat}}\ h)^{-1}$.

hydrogen was adsorbed on the Cu surface and dissociated into hydrogen atoms. Secondly, hydrogen atoms arrived at the ZnO and ZnO_x surface on the interface of Cu–Zn by hydrogen spill-over effect to react with CO_2 adsorbed on ZnO and ZnO_x. Finally, methanol was generated on ZnO_x through a series of intermediate, and CO was produced on ZnO.

The most efficient CZ-2 catalyst was selected for a stability test, and the result was presented in Fig. 8. The conversion of CO_2 and the selectivity of methanol decreased slightly during the continuous 100 h, indicating that the CZ catalysts prepared by *in situ* chemical reduction reaction involved impregnation of cylindrical shaped ZnO with Cu^{2+} aqueous solution had a stable catalytic performance for CO_2 hydrogenation to methanol.

4. Conclusions

The cylindrical shaped ZnO was synthesized by hydrothermal process. Four Cu/ZnO catalysts were prepared *via in situ* chemical reduction reaction between Cu^{2+} and L-ascorbic acid involved impregnation of cylindrical shaped ZnO with Cu^{2+} aqueous solution. For comparison, the catalyst prepared by carbonate coprecipitation was also synthesized. The physico-chemical properties and catalytic activity of the catalysts are strongly influenced by the Cu content. With the increase in Cu/Zn molar ratio, the BET surface area and exposed Cu surface area exhibited a volcanic shaped curve, and the polarity of ZnO decreased. The CZ-2 catalyst had the highest exposed Cu surface area and more oxygen vacancies, which exhibited an optimum catalytic activity. This observation indicates that the CO_2 conversion is correlated with the amount of chemisorbed hydrogen. The methanol selectivity decreased with reduction of oxygen vacancies in ZnO, which suggested that active sites for methanol and CO were different, and oxygen vacancies were active sites for methanol. No activity for methanol was observed on pure Cu, which showed clearly that the Cu–Zn synergy had a very critical role in the methanol formation. CZ-2 catalyst exhibited the superior catalytic performance than CZ-CC obtained by conventional coprecipitation method. This method is a promising way for preparation of highly effective Cu/ZnO catalysts.

Conflicts of interest

There are no conflicts to declare.

Acknowledgements

This work was financially supported by Basic Public Welfare Research Project of Zhejiang (grant number LGG18B020003), Science and Technology Project of Quzhou (grant number 2016Y005), National College Students Innovation Project of China (grant number 201711488017).

References

1 A. Goeppert, M. Czaun, J. P. Jones, G. K. S. Prakash and G. A. Olah, *Chem. Soc. Rev.*, 2014, **43**, 7995–8048.
2 H. B. Song, N. Zhang, C. Y. Zhong, Z. Liu, M. Xiao and H. J. Gai, *New J. Chem.*, 2017, **41**, 9170–9177.
3 P. De Luna, R. Q. Bermudez, C. T. Dinh, M. B. Ross, O. S. Bushuyev, P. Todorović, T. Regier, S. O. Kelley, P. d. Yang and E. H. Sargent, *Nat. Catal.*, 2018, **1**, 103–110.
4 G. T. Zeng, J. Qiu, Z. Li, P. Pavaskar and S. B. Cronin, *ACS Catal.*, 2014, **4**, 3512–3516.
5 G. O. Olah, A. Goeppert and G. K. S. Prakash, *J. Org. Chem.*, 2009, **74**, 487–498.
6 X. M. Guo, D. S. Mao, G. Z. Lu, S. Wang and G. S. Wu, *Catal. Commun.*, 2011, **12**, 1095–1098.
7 F. L. Liao, Y. Q. Huang, J. W. Ge, W. R. Zheng, K. Tedsree, P. Collie, X. L. Hong and S. C. Tsang, *Angew. Chem.*, 2011, **123**, 2210–2213.
8 P. Gao, F. Li, F. K. Xiao, N. Zhao, N. N. Sun, W. Wei, L. S. Zhong and Y. H. Sun, *Catal. Sci. Technol.*, 2012, **2**, 1447–1454.
9 Y. Jiang, H. Y. Yang, P. Gao, X. P. Li, J. M. Zhang, H. J. Liu, H. Wang, W. Wei and Y. H. Sun, *J. CO2 Util.*, 2018, **26**, 642–651.
10 F. Arena, G. Mezzatesta, G. Zafarana, G. Trunfio, F. Frusteri and L. Spadaro, *J. Catal.*, 2013, **300**, 141–151.
11 H. Lei, R. F. Nie, G. Q. Wu and Z. Y. Hou, *Fuel*, 2015, **154**, 161–166.
12 S. Kuld, M. Thorhauge, H. Falsig, C. F. Elkjær, S. Helveg, I. Chorkendorff and J. Sehested, *Science*, 2016, **352**, 969–974.
13 S. Kattel, P. J. Ramírez, J. G. Chen, J. A. Rodriguez and P. Liu, *Science*, 2017, **355**, 1296–1299.
14 S. Kuld, C. Conradsen, P. G. Moses, I. Chorkendorff and J. Sehested, *Angew. Chem., Int. Ed.*, 2014, **53**, 5941–5945.
15 F. Frusteri, M. Cordaro, C. Cannilla and G. Bonura, *Appl. Catal., B*, 2015, **162**, 57–65.
16 F. Arena, K. Barbera, G. Italiano, G. Bonura, L. Spadaro and F. Frusteri, *J. Catal.*, 2007, **249**, 185–194.
17 N. Mota, R. Guil-Lopez, B. G. Pawelec, J. L. G. Fierro and R. M. Navarro, *RSC Adv.*, 2018, **8**, 20619–20629.
18 H. Jeong, C. H. Cho and T. H. Kim, *React. Kinet., Mech. Catal.*, 2012, **106**, 435–443.
19 S. A. Kondrat, P. J. Smith, P. P. Wells, P. A. Chater, J. H. Carter, D. J. Morgan, E. M. Fiordaliso, J. B. Wagner, T. E. Davies, L. Lu, J. K. Bartley, S. H. Taylor, M. S. Spencer, C. J. Kiely, G. J. Kelly, C. W. Park, M. J. Rosseinsky and G. J. Hutchings, *Nature*, 2016, **531**, 83–87.
20 A. Karelovic, A. Bargibant, C. Fernández and P. Ruiz, *Catal. Today*, 2012, **197**, 109–118.
21 A. Le Valant, C. Comminges, C. Tisseraud, C. Canaff, L. Pinard and Y. Pouilloux, *J. Catal.*, 2015, **324**, 41–49.
22 T. Witoon, T. Permsirivanich, W. Donphai, A. Jaree and M. Chareonpanich, *Fuel Process. Technol.*, 2013, **116**, 72–78.
23 J. Schumann, M. Eichelbaum, T. Lunkenbein, N. Thomas, M. C. Á. Galvan, R. Schlögl and M. Behrens, *ACS Catal.*, 2015, **5**, 3260–3270.
24 A. A. Khassin, V. V. Pelipenko, T. P. Minyukova, V. I. Zaikovskii, D. I. Kochubey and T. M. Yurieva, *Catal. Today*, 2006, **112**, 143–147.

25 M. Kurtz, N. Bauer, C. Büscher, H. Wilmer, O. Hinrichsen, R. Becker, S. Rabe, K. Merz, M. Driess, R. A. Fischer and M. Muhler, *Catal. Lett.*, 2004, **92**, 49–52.
26 M. Peter, M. B. Fichtl, H. Ruland, S. Kaluza, M. Muhler and O. Hinrichse, *Chem. Eng. J.*, 2012, **203**, 480–491.
27 S. D. Senanayake, P. J. Ramírez, I. Waluyo, S. Kundu, K. Mudiyanselage, Z. Y. Liu, Z. Liu, S. Axnanda, D. J. Stacchiola, J. Evans and J. A. Rodriguez, *J. Phys. Chem. C*, 2016, **120**, 1778–1784.
28 M. B. Fichtl, J. Schumann, I. Kasatkin, N. Jacobsen, M. Behrens, R. Schlögl, M. Muhler and O. Hinrichsen, *Angew. Chem., Int. Ed.*, 2014, **53**, 7043–7047.
29 P. K. Khanna, T. S. Kale, M. Shaikh, N. K. Rao and C. V. V. Satyanarayana, *Mater. Chem. Phys.*, 2008, **110**, 21–25.
30 G. C. Chinchen, C. M. Hay, H. D. Vandervell and K. C. Waugh, *J. Catal.*, 1987, **103**, 79–86.
31 S. Lee, K. Schneider, J. Schumann, A. Mogalicherla, P. Pfeifer and R. Dittmeyer, *Chem. Eng. Sci.*, 2015, **138**, 194–202.
32 G. R. Li, T. Hu, G. L. Pan, T. Y. Yan, X. P. Gao and H. Y. Zhu, *J. Phys. Chem. C*, 2008, **112**, 11859–11864.
33 J. Iqbal, N. Safdar, T. Jan, M. Ismail, S. S. Hussain, A. Mahmood, S. Shahzad and Q. Mansoor, *J. Mater. Sci. Technol.*, 2015, **31**, 300–304.
34 Y. G. Lin, Y. K. Hsu, S. Y. Chen, L. C. Chen and K. H. Chen, *J. Mater. Chem.*, 2011, **21**, 324–326.
35 M. Chen, X. Wang, Y. Yu, Z. Pei, X. Bai, C. Sun, R. Huang and L. Wen, *Appl. Surf. Sci.*, 2000, **158**, 134–140.
36 J. C. Fan and J. B. Goodenough, *J. Appl. Phys.*, 1977, **48**, 3524–3531.
37 J. Pritchard, T. Catterick and R. K. Gupta, *Surf. Sci.*, 1975, **53**, 1–20.
38 M. S. Spencer, *Top. Catal.*, 1999, **8**, 259–266.
39 P. Gao, F. Li, N. Zhao, F. K. Xiao, W. Wei, L. S. Zhong and Y. H. Sun, *Appl. Catal., A*, 2013, **468**, 442–452.
40 L. C. Wang, Q. Liu, M. Chen, Y. M. Liu, Y. Cao, H. Y. He and K. N. Fan, *J. Phys. Chem. C*, 2007, **111**, 16549–16557.
41 H. Lei, Z. Y. Hou and J. W. Xie, *Fuel*, 2016, **164**, 191–199.